Nonlinear Power Loss During Exercise in Single-Ventricle Patients After the Fontan: Insights From Computational Fluid Dynamics

Kevin K. Whitehead, Kerem Pekkan, Hiroumi D. Kitajima, Stephen M. Paridon, Ajit P. Yoganathan and Mark A. Fogel

Circulation 2007;116;I-165-I-171
DOI: 10.1161/CIRCULATIONAHA.106.680827
Circulation is published by the American Heart Association. 7272 Greenville Avenue, Dallas, TX 72514
 Print ISSN: 0009-7322. Online ISSN: 1524-4539

Nonlinear Power Loss During Exercise in Single-Ventricle Patients After the Fontan

Insights From Computational Fluid Dynamics

Kevin K. Whitehead, MD, PhD; Kerem Pekkan, PhD; Hiroumi D. Kitajima, MS; Stephen M. Paridon, MD; Ajit P. Yoganathan, PhD; Mark A. Fogel, MD

Background—We previously demonstrated that power loss (PL) through the total cavopulmonary connection (TCPC) in single-ventricle patients undergoing Fontan can be calculated by computational fluid dynamic analysis using 3-dimensional MRI anatomic reconstructions. PL through the TCPC may play a role in single-ventricle physiology and is a function of cardiac output. We hypothesized that PL through the TCPC increases significantly under exercise flow conditions.

Methods and Results—MRI data of 10 patients with a TCPC were analyzed to obtain 3-dimensional geometry and flow rates through the superior vena cava, inferior vena cava, left pulmonary artery, and right pulmonary artery. Steady computational fluid dynamic simulations were performed at baseline conditions using MRI-derived flows. Simulated exercise conditions of twice (2×) and three times (3×) baseline flow were performed by increasing inferior vena cava flow. PL, head loss, and effective resistance through the TCPC were calculated for each condition. Each condition was repeated at left pulmonary artery/right pulmonary artery ratios of 30/70 and 70/30 to determine the effects of pulmonary flow splits on exercise PL. For each patient, PL increases dramatically in a nonlinear fashion with increasing cardiac output, even when normalized to calculate head loss or resistance. Flow splits had a significant effect on PL at exercise, with most geometries favoring right pulmonary artery flow.

Conclusions—The relationship between cardiac output and PL is nonlinear and highly dependent on TCPC geometry and pulmonary flow splits. This study demonstrates the importance of studying the TCPC under exercise conditions, because baseline conditions may not adequately characterize TCPC efficiency. **(*Circulation*. 2007;116[suppl I]:I-165–I-171.)**

Key Words: blood flow ■ computational fluid dynamics ■ exercise ■ Fontan procedure ■ hemodynamics ■ magnetic resonance imaging

For 30 years, the Fontan procedure and its modifications have been the standard end point for most single-ventricle patients. Despite improvements in surgical strategies and management, these patients still face high mortality and morbidity and decreased quality of life compared with peers,[1] including limited exercise capacity compared with age-matched normal subjects.[2–5] The etiology of this decreased exercise capacity is unclear. The past few years have seen a focus on characterizing power loss through the total cavopulmonary connection (TCPC).[6–10] We hypothesize that TCPC efficiency plays a significant role in the exercise capacity of Fontan patients. Previous work has demonstrated significant effects of TCPC geometry on power loss.[10–13] This power loss can be amplified by increasing the flow through the TCPC.[14] It follows that a TCPC geometry with greater power loss or whose power loss increases more with exercise may have a decreased ability to increase TCPC flow during exercise. This in turn would result in decreased capacity for oxygen delivery during exercise and thus decreased exercise performance. Likewise, a patient with a more efficient TCPC may have a greater ability to exercise.

Recent studies have focused on the Fontan circulation under resting conditions.[8,12,13,15] Some studies have evaluated a range of flow conditions that are not necessarily representative of physiological flows under exercise. The goal of this study was to evaluate power loss in a group of TCPC patients using previously validated computational fluid dynamic techniques under baseline and exercise conditions to gain a better understanding of the effects of exercise on TCPC power loss. A secondary goal was to determine the effect of varying relative flow to each lung on the power loss in the TCPC under exercise conditions. If differences in power loss for

From the Division of Cardiology (K.K.W., S.M.P., M.A.F.), Children's Hospital of Philadelphia, Philadelphia, Pa; the Cardiovascular Fluid Mechanics Laboratory, Wallace H. Coulter Department of Biomedical Engineering (H.D.K., A.P.Y.), Georgia Institute of Technology, Atlanta, Ga; the Biomedical Engineering Department (K.P.), Carnegie Mellon University, Pittsburgh, Pa.

Presented at the American Heart Association Scientific Sessions, Chicago, Ill, November 12–15, 2006.

Correspondence to Kevin K. Whitehead, MD, PhD, Children's Hospital of Philadelphia, Cardiology, Main Hospital, 2nd Floor, 34th and Civic Center Blvd, Philadelphia, PA 19104. E-mail whiteheadk@email.chop.edu.

Circulation **is available at http://circ.ahajournals.org** **DOI: 10.1161/CIRCULATIONAHA.106.680827**

different flow splits to the pulmonary arteries are magnified at exercise conditions, this could result in either changes in relative pulmonary blood flow or in additional inefficiencies of the TCPC. If flow splits remain the same with exercise, as suggested by studies from Pedersen et al,[16] but the optimal flow split for minimizing power loss is different, this could result in further TCPC inefficiencies.

Methods

A multicenter Fontan patient MRI database has been assembled to study the anatomic elements of the TCPC. Informed consent was obtained and all associated studies approved by the Internal Review Boards of the Children's Hospital of Philadelphia (CHOP) and Georgia Institute of Technology. Ten geometries were selected from the CHOP cohort that had adequate anatomic and velocity data to perform valid simulations. Inclusion criteria included: (1) the anatomic reconstruction had no significant visible artifacts or holes in it, and (2) velocity data were available for all caval veins and left and right pulmonary arteries. The authors had full access to and take full responsibility for the integrity of the data. All authors have read and agree to the article as written.

Anatomic and Flow Data

Previous reconstructions of 3-dimensional patient-specific morphologies from MRI have enabled detailed and realistic flow analyses.[17] The anatomic models are obtained from patient MRI contiguous axial stacks of steady-state free-precession data. Typical scans have in-plane resolutions of 1.0 to 1.5 mm and out-of-plane (slice thickness) resolutions of 3 to 5 mm. Electrocardiographic gating was performed to obtain all images in end-diastole. Out-of-plane image resolution is enhanced with an adaptive control grid interpolation technique to produce isotropic voxels.[18] Each TCPC is isolated within the enhanced MRI data using a shape-element segmentation technique. Intensity thresholding and edge detection methods are used to create a scaffold around the TCPC, within which the vascular area of interest is defined by the motion of a shape element. Computer-aided design tools are used to produce a 3-dimensional model of the TCPC from the segmented data. The resulting geometry is locally smoothed and gaps filled if required.

Using phase contrast through-plane velocity mapping, flow rates from each vessel supplying and draining the region of cavopulmonary connection are measured. Using these velocity maps, baseline resting flow rates are calculated.

Computational Simulation

The 3-dimensional anatomic reconstructions are used for grid generation in which vessel volumes are divided into computational elements (meshes). The number of elements varies depending on geometry size and complexity, but ranges from 548 842 to 1 674 440 for the models studied. At each element, the governing Navier-Stokes conservation equations of mass and momentum for laminar fluid flow are solved. All solutions were obtained using second-order solvers assuming a Newtonian fluid with a density of 1060 kg/m^3 and viscosity of 3.71e-3 N-s/m^2. The patient-specific TCPC computational fluid dynamic analysis methodology and the in vitro validations of these techniques have been described elsewhere[19] and are further detailed in the online supplement.

Flow Conditions

Each patient geometry was simulated at baseline steady-state flow conditions by setting the caval vessel flows at a steady rate derived from the MRI flow data averaged over the cardiac cycle. To satisfy conservation of mass, left pulmonary artery (LPA) and right pulmonary artery (RPA) flows were set to a fraction of total caval flow corresponding to the MRI-measured pulmonary flow splits. Exercise simulations of 2 (2×) and 3 times (3×) baseline total flows were performed to simulate exercise flows. This is partially justified by limited data from Shachar et al, in which Fontan patients had significantly depressed baseline cardiac output compared with normal control subjects but were on average able to increase their cardiac index by 2.1 times baseline.[5] RPA/LPA flow splits were assumed to remain the same.[16] Our exercise simulations were intended to simulate lower limb exercise and assumed that all increases in caval blood flow are from the inferior vena cava (IVC). This has been shown to be the case in normal subjects.[20] Limited studies indicate that the caval blood flow changes in Fontan patients in response to exercise are similar.[16,21] In the one patient with interrupted IVC with azygous continuation (CHOP20), increased flow from the lower body was split proportionally, according to the baseline measurements, between the azygous vein and the hepatic vein to the pulmonary artery pathway.

To investigate the effect of pulmonary flow split on exercise hemodynamics, we repeated each condition with 30% and 70% of flow to the LPA. Note that these simulations are not to imply that these are realistic flows for a given geometry. It would be unlikely for 70% of pulmonary blood flow to go through a stenotic vessel. However, these data allow us to calculate equal vascular lung resistance (EVLR) operating points. The method for this has been described elsewhere[13] and is detailed in the online supplement.

Power Loss Calculations

To characterize TCPC efficiency under baseline and exercise conditions, power loss through the TCPC was calculated using the control volume method derived from the macroscopic energy balance:

$$\dot{E} = \int_{Surface} \left[p + \frac{1}{2}\rho u_j u_j \right] u_j n_j dS \cong \left(p + \frac{1}{2}\rho v^2 \right) Q \Big|$$

This has been described more thoroughly in previous work[22] and is detailed in the online supplement. In practical terms, total power for each surface is calculated by summing the inertial and static components. From this, net power loss is calculated by subtracting outlet power from inlet power:

$$\dot{E}_{delta} = \dot{E}_{SVC} + \dot{E}_{IVC} - \dot{E}_{lpa} - \dot{E}_{rpa}$$

where $\dot{E}_{delta}$ is the net power loss in the control volume.

Results

Patient demographics, pulmonary artery dimensions at the position of flow measurement, measured flows, and MRI-measured and calculated EVLR baseline flow splits are summarized in the Table. Figure 1 summarizes calculated power loss versus exercise condition for all 10 geometries studied. Note power loss increases nonlinearly with increasing flow with an average increase of 10.5 times and 38.9 times baseline to the 2× and 3× exercise conditions, respectively. Power loss normalized to cardiac output (effective head loss) shows a similar trend (Figure 2). Further indexing of head loss by cardiac index (Figure 2) demonstrates that resistance index increases with flow. Although slight inaccuracies may be exaggerated, the calculated increases do not seem unreasonable because hydraulic power loss is proportional to flow times pressure loss, and pressure losses attributable to the dissipation of kinetic energy are themselves related to the square of velocity, a relationship familiar to cardiologists who use the modified Bernoulli equation.

Flow Visualization

Flow fields from CHOP31 are presented in Figure 3. At baseline, a vortex forms centrally with some penetration of IVC flow into the superior vena cava (SVC). As cardiac output increases, SVC–IVC flow collision is much more

Summary of Demographic, Flow, and Pulmonary Artery Cross-Sectional Area for Each Patient in the Study*

Patient	Age, y	Body Surface Area, m^2	SVC, L/min	IVC, L/min	Percent to LPA	EVLR (% to LPA) Rest	EVLR (% to LPA) Ex3	CI, L/min/m^2	Cross-Sectional Area LPA, cm^2	Cross-Sectional Area RPA, cm^2
CHOP18	11.3	1.23	0.93	2.17	41	31	27	2.52	0.58	1.64
CHOP20	12.7	1.22	0.38	2.57	42	56	61	2.42	2.61	1.72
CHOP22	9.9	1.01	1.20	1.75	58	45	42	2.92	1.20	1.24
CHOP25	18.1	1.58	0.91	2.83	36	37	31	2.37	1.47	2.94
CHOP30	11.0	1.32	1.52	2.28	55	49	50	2.87	1.86	1.76
CHOP31	14.5	1.89	0.89	4.15	43	42	37	2.67	2.43	2.55
CHOP32	18.3	2.01	2.00	4.97	28	47	45	3.47	4.13	4.67
CHOP33	8.8	0.69	1.23	2.29	62	44	33	5.10	1.79	2.31
CHOP34	11.3	1.19	1.93	3.31	55	43	35	4.40	2.67	1.78
CHOP37	17.7	1.49	1.04	3.06	56	64	69	2.75	2.89	1.51

*Patients are referred to by their code in the Fontan database throughout the article.
Ex3 indicates 3x exercise condition; CI, Cardiac Index.

striking with significant power loss occurring in this region. In the orthogonal view, one can appreciate an additional source of power loss at exercise conditions from a narrowing in the IVC baffle. Complete flow fields for all 10 patient geometries are presented in the Appendix.

Effect of Pulmonary Flow Splits

Figure 4 summarizes the effect of varying LPA flow from 30% to 70% for 4 representative patient geometries. For most, increasing LPA flow for a given cardiac output leads to increased power loss, an effect magnified at exercise. One geometry (CHOP37) demonstrated marked preference toward the LPA. Not surprisingly, this model had a larger relative LPA size with mild proximal RPA hypoplasia. The power losses of some geometries (CHOP22, CHOP30, CHOP20) are relatively independent of pulmonary flow split. Figure 5 summarizes the effect of pulmonary flow splits on the 3× exercise condition with EVLR points marked by stars.

Discussion

Effect of Exercise

We demonstrated that power loss in the TCPC increases markedly and in a nonlinear fashion with increasing flow. More importantly, power loss normalized to calculate an effective resistance index still demonstrated flow rate dependence. TCPC resistance at the 3× exercise condition was as high as 3.4 mm Hg/[L/min/m^2], which is on the order of magnitude of the pulmonary vascular resistance.

This dramatic increase in resistance index with exercise may cause significant increases in Fontan baffle pressure, limiting TCPC flow during exercise. Head losses in Figure 2 at the 3×

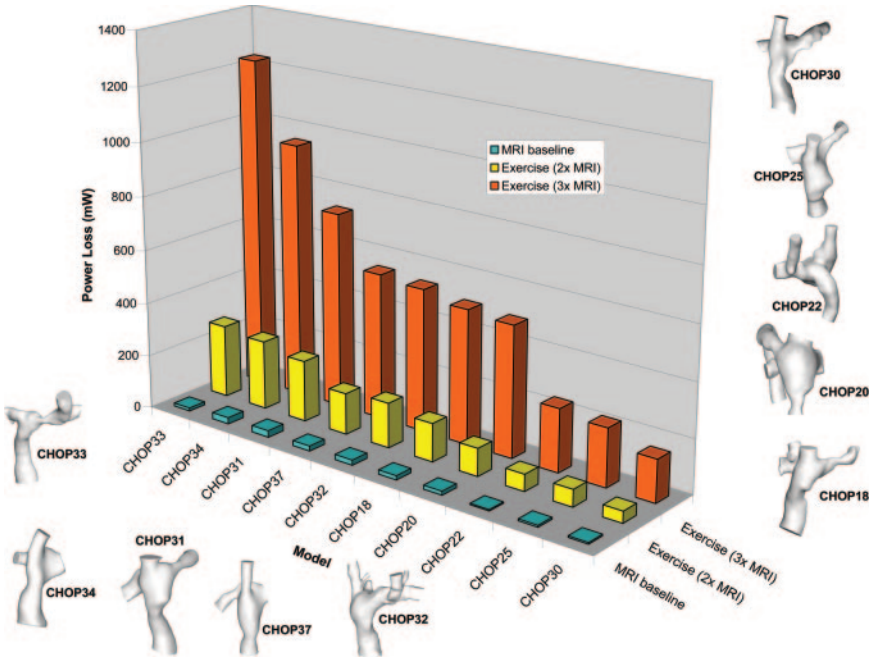

Figure 1. Chart showing power loss as a function of flow condition (baseline MRI flow conditions, 2× MRI exercise condition, and 3× MRI exercise condition) for all 10 patient geometries arranged by maximum power loss. Images: grayscale images of patient geometries studied.

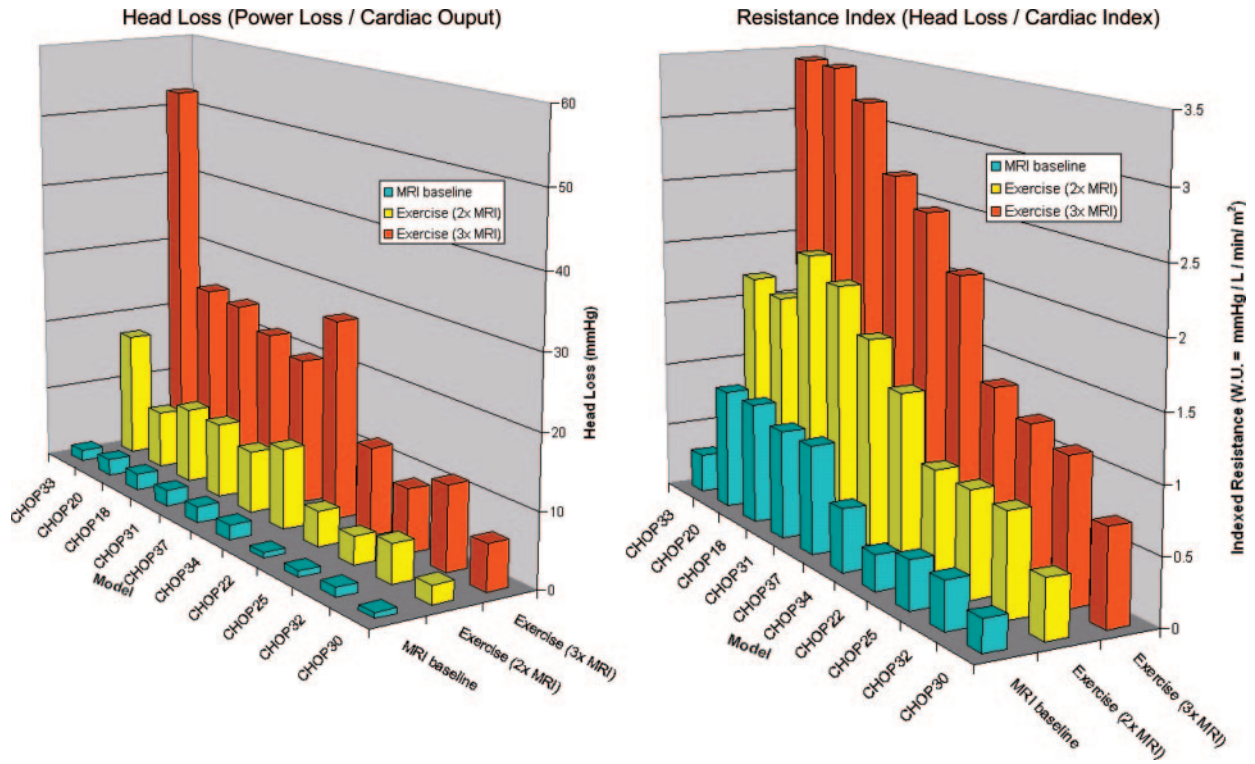

Figure 2. Left: Head loss (power loss normalized to cardiac output). Right: resistance index (head loss normalized to cardiac index).

MRI flow exercise condition are nonphysiological for many patient geometries corresponding to pressure drops of as high as 52 mm Hg. Although other factors such as pulmonary vascular resistance and ventricular filling are likely important, this may partially explain why most Fontan patients are unable to obtain this level of exercise performance.

Effect of Pulmonary Flow Splits

Another significant phenomenon explored was the effect of pulmonary flow splits on power loss. For most geometries, power loss increased significantly as LPA flow increased, reflecting LPA hypoplasia. Although the penalty for increasing LPA flow was generally small at

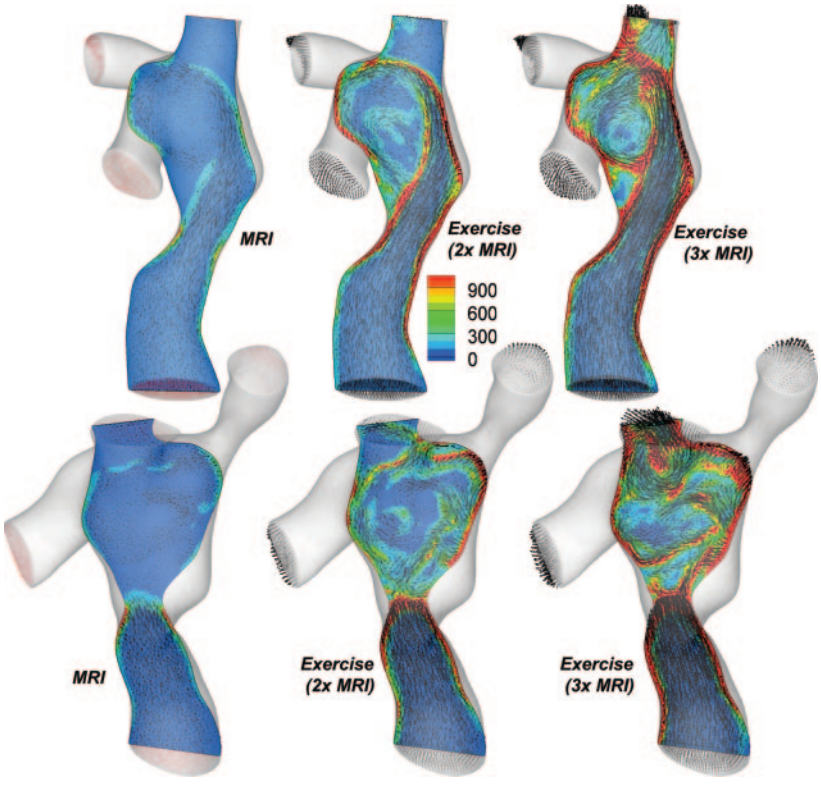

Figure 3. Flow features for model CHOP31 at the 3 flow conditions: baseline MRI, and 2× and 3× baseline exercise conditions. Note the increased flow collision and power dissipation (mW) in region of SVC with increased flow (upper) and power loss at the narrowing of the IVC (lower).

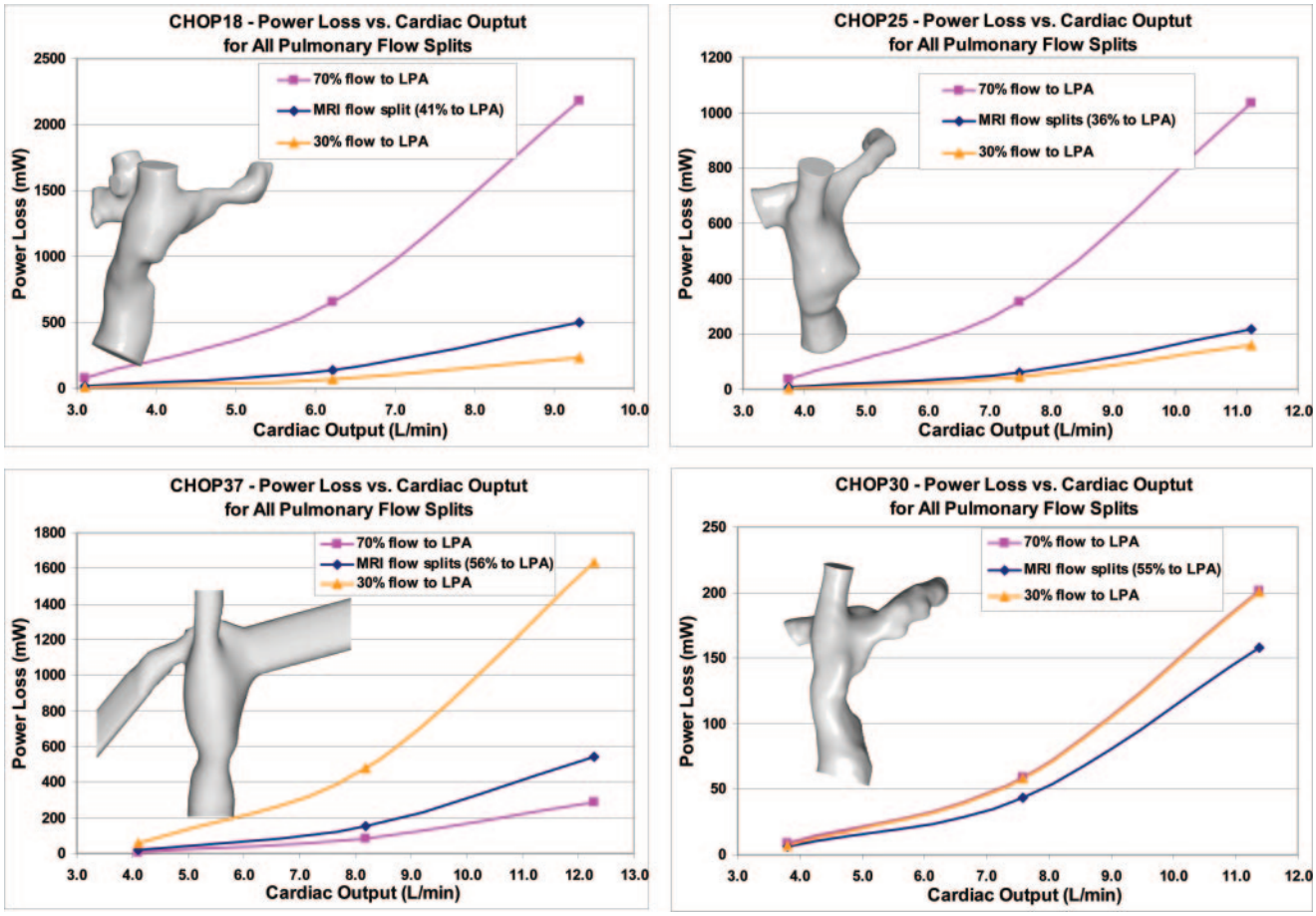

Figure 4. Effects of pulmonary flow splits on power loss in 4 representative patient geometries. CHOP18 and CHOP25 demonstrate increased power loss with increased flow to the LPA, whereas CHOP37 demonstrates the opposite trend. CHOP30 is relatively insensitive to pulmonary flow splits.

baseline flows, it was quite significant at exercise. It has been shown that IVC flow is directed toward the LPA and SVC flow toward the RPA.[23] Increasing IVC flow to simulate exercise forces more blood through the LPA or forces abnormal streaming of IVC flow into the RPA.

Note in the Table the variability in the EVLR point at baseline flows. Furthermore, the EVLR point changes by as much as 10% from baseline to exercise, suggesting that TCPC geometry plays an important role in pulmonary flow distribution at both rest and exercise.

Flow Visualization

Flow visualization from our computational simulations (Figure 3; Appendix) demonstrates the importance of collision between the SVC and IVC flow during exercise. In our simulations, many of the geometries demonstrate increased penetrance of IVC flow into the SVC with exercise flow rates attributable to increased IVC flow and momentum. This results in increased power loss and thus decreased efficiency of the TCPC during exercise.

Preliminary Clinical Correlation

The ultimate goal of this research is to establish the clinical importance of power loss through the TCPC. In 7 of the patient geometries studied, we had adequate metabolic exercise studies (as defined by a Respiratory Exchange Ratio of greater than 1.1). Figure 6 shows a plot of the percent of predicted maximum oxygen consumption (O_2) versus the resistance index at the 3× flow condition for these 7 patients. Note that the trend is negative but that the sample size is insufficient to be significant. The goal of future research will be to obtain a large enough sample size to determine whether the effects of increased flow rate on power loss demonstrated in this study have a significant clinical impact on exercise performance.

Previous Studies

Although TCPC power loss is recognized as a potentially important factor in the long-term outcome of Fontan patients, most studies have focused on resting conditions. Hsia et al studied computational fluid dynamic models reconstructed from angiographic data under resting conditions, showing that idealized extracardiac models had lower power loss than lateral tunnel or intraatrial tube connections.[8] Migliavacca et al studied 3-dimensional models derived from MRI data. They again focused on different TCPC types under MRI-measured resting flow conditions, studying 4 intraatrial and 2 extracardiac geometries with variations in the IVC anastomosis, showing that IVC size and anastomosis geometry significantly affect power dissipation.[12]

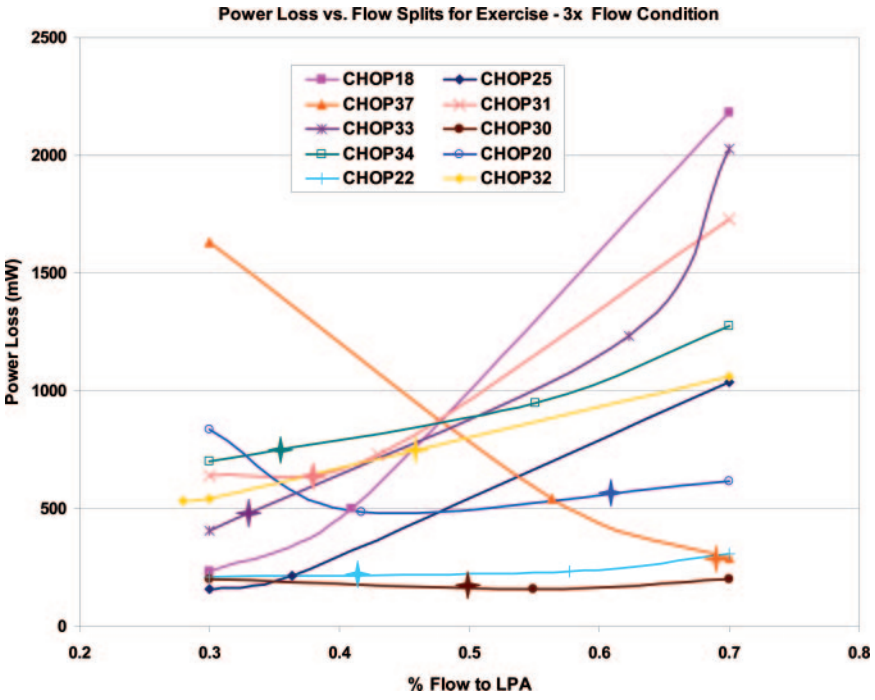

Figure 5. Power loss at the 3× baseline flow condition versus percent pulmonary flow to LPA for each geometry.

Some studies have varied flow rate, but none systematically examined the effect of physiological exercise flow rates on TCPC efficiency. De Zelicourt et al studied a TCPC with bilateral SVCs under varying pulmonary flow splits and flows. Flows were changed by increasing IVC and SVC flows symmetrically as opposed to increasing only the IVC. They concluded that power losses were reduced by moving the IVC anastomosis more centrally.[14]

Limitations

Although great care was made to accurately reconstruct the geometry, it is conceivable that some stenoses may be exaggerated, which may in turn exaggerate the effects of exercise for some models. The proportions of flow through the different sections of each model were not necessarily realistic, particularly when flow that could have found an alternative route was forced through a stenosed section. For example, the pulmonary artery stenosis located between the IVC flow path and the entry of a left-sided SVC in CHOP33 carried little flow and caused insignificant power loss at baseline, but appeared to result in a 99-fold increase of power loss in the exercising condition. In a patient, however, increased flow through the right lung or through azygos venous collaterals to the left could bypass the stenosis on exertion. However, because nonlinear effects of exercise were observed in all models, it is unlikely that these exaggerations would affect the overall results.

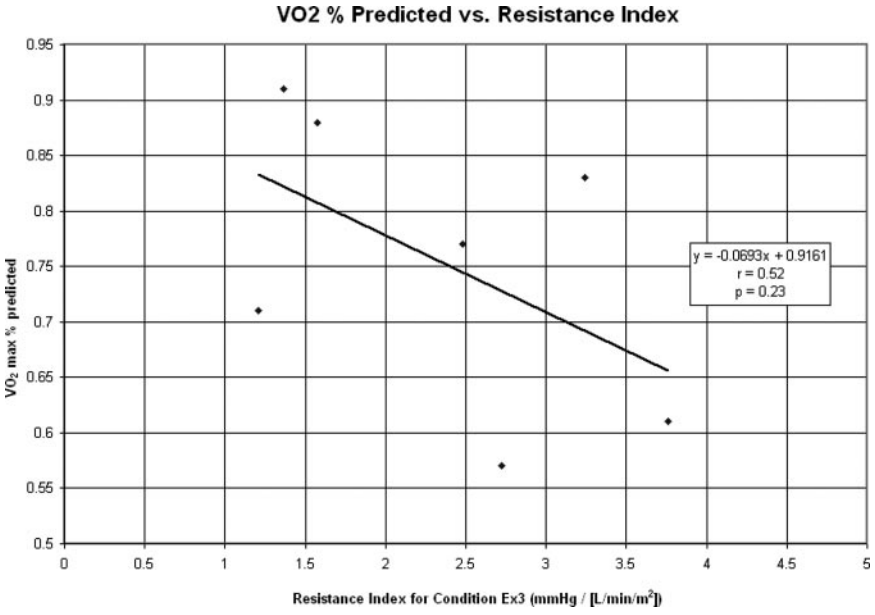

Figure 6. Percent predicted maximum oxygen consumption versus resistance index at the 3× baseline condition for the 7 patients with adequate metabolic exercise tests. Note the negative trend, but the correlation is not significant given the small sample size.

Another significant limitation is the use of rigid models. This is an area of active investigation, but preliminary studies indicate that compliance effects are on the order of 9% to 15%.[24] We would expect these effects to be similar across all models studied, making comparisons between models valid. Ignoring the small pulsatile component of caval flow may cause small overestimations in power loss, which again should be similar across the models.

A third important limitation is the use of laminar simulations. At the highest flow rates, there may be some regional areas of turbulence. In this case, the calculated power loss would underestimate actual power loss, making exercise effects even more important than demonstrated in these simulations.

Conclusions

Power loss increases in a nonlinear fashion with physiological increases in IVC flow simulating lower limb exercise. Small differences in power loss between patients at rest may translate into marked, hemodynamically important differences at exercise. In addition, relative pulmonary blood flow to each lung at exercise has a profound effect on power loss. It may be important to understand the effect of exercise on pulmonary blood flow distribution to adequately characterize TCPC efficiency.

Future studies will be aimed at exploring the differences between the flow characteristics of extracardiac and lateral tunnel Fontans under both resting and exercise conditions. We will continue to explore the clinical relevance of these findings by comparing the hydrodynamic analysis presented in this research with actual patient metabolic exercise data in a larger series of patients. The ultimate goal is to provide guidelines and tools for surgeons to optimize the TCPC pathway.

Sources of Funding

This work was supported by NIH BRP Grant R01 HL 67622 from the National Heart, Lung and Blood Institute. K.K.W. was supported in part by the NIH training grant T32 HL007915–08.

Disclosure

None.

References

1. Mair DD, Puga FJ, Danielson GK. The Fontan procedure for tricuspid atresia: early and late results of a 25-year experience with 216 patients. *J Am Coll Cardiol*. 2001;37:933–939.
2. Brassard P, Bedard E, Jobin J, Rodes-Cabau J, Poirier P. Exercise capacity and impact of exercise training in patients after a Fontan procedure: a review. *Can J Cardiol*. 2006;22:489–495.
3. Ohuchi H, Arakaki Y, Hiraumi Y, Tasato H, Kamiya T. Cardiorespiratory response during exercise in patients with cyanotic congenital heart disease with and without a Fontan operation and in patients with congestive heart failure. *Int J Cardiol*. 1998;66:241–251.
4. Rosenthal M, Bush A, Deanfield J, Redington A. Comparison of cardiopulmonary adaptation during exercise in children after the atriopulmonary and total cavopulmonary connection Fontan procedures. *Circulation*. 1995;91:372–378.
5. Shachar GB, Fuhrman BP, Wang Y, Lucas RV Jr, Lock JE. Rest and exercise hemodynamics after the Fontan procedure. *Circulation*. 1982; 65:1043–1048.
6. Ensley AE, Ramuzat A, Healy TM, Chatzimavroudis GP, Lucas C, Sharma S, Pettigrew R, Yoganathan AP. Fluid mechanic assessment of the total cavopulmonary connection using magnetic resonance phase velocity mapping and digital particle image velocimetry. *Annals of Biomedical Engineering*. 2000;28:1172–1183.
7. Healy TM, Lucas C, Yoganathan AP. Noninvasive fluid dynamic power loss assessments for total cavopulmonary connections using the viscous dissipation function: a feasibility study. *J Biomech Eng*. 2001;123: 317–324.
8. Hsia TY, Migliavacca F, Pittaccio S, Radaelli A, Dubini G, Pennati G, de Leval MR. Computational fluid dynamic study of flow optimization in realistic models of the total cavopulmonary connections. *J Surg Res*. 2004;116:305–313.
9. Moyle KR, Mallinson GD, Occleshaw CJ, Cowan BR, Gentles TL. Wall shear stress is the primary mechanism of energy loss in the Fontan connection. *Pediatr Cardiol*. 2006;27:309–315.
10. Ryu K, Healy TM, Ensley AE, Sharma S, Lucas C, Yoganathan AP. Importance of accurate geometry in the study of the total cavopulmonary connection: computational simulations and in vitro experiments. *Ann Biomed Eng*. 2001;29:844–853.
11. Khunatorn Y, Mahalingam S, DeGroff CG, Shandas R. Influence of connection geometry and SVC–IVC flow rate ratio on flow structures within the total cavopulmonary connection: a numerical study. *J Biomech Eng*. 2002;124:364–377.
12. Migliavacca F, Dubini G, Bove EL, de Leval MR. Computational fluid dynamics simulations in realistic 3-D geometries of the total cavopulmonary anastomosis: the influence of the inferior caval anastomosis. *J Biomech Eng*. 2003;125:805–813.
13. Pekkan K, Kitajima HD, de Zelicourt DA, Forbess JM, Parks WJ, Fogel MA, Sharma S, Kanter KR, Frakes D, Yoganathan AP. Total cavopulmonary connection flow with functional left pulmonary artery stenosis: angioplasty and fenestration in vitro. *Circulation*. 2005;112: 3264–3271.
14. de Zelicourt DA, Pekkan K, Parks J, Kanter K, Fogel M, Yoganathan AP. Flow study of an extracardiac connection with persistent left superior vena cava. *J Thorac Cardiovasc Surg*. 2006;131:785–791.
15. Migliavacca F, de Leval MR, Dubini G, Pietrabissa R, Fumero R. Computational fluid dynamic simulations of cavopulmonary connections with an extracardiac lateral conduit. *Med Eng Phys*. 1999;21:187–193.
16. Pedersen EM, Stenbog EV, Frund T, Houlind K, Kromann O, Sorensen KE, Emmertsen K, Hjortdal VE. Flow during exercise in the total cavopulmonary connection measured by magnetic resonance velocity mapping. *Heart*. 2002;87:554–558.
17. de Zelicourt DA, Pekkan K, Wills L, Kanter K, Forbess J, Sharma S, Fogel M, Yoganathan AP. In vitro flow analysis of a patient-specific intraatrial total cavopulmonary connection. *Ann Thorac Surg*. 2005;79: 2094–2102.
18. Frakes DH, Conrad CP, Healy TM, Monaco JW, Fogel M, Sharma S, Smith MJ, Yoganathan AP. Application of an adaptive control grid interpolation technique to morphological vascular reconstruction. *IEEE Trans Biomed Eng*. 2003;50:197–206.
19. Pekkan K, de Zelicourt DA, Ge L, Sotiropoulos F, Frakes D, Fogel MA, Yoganathan AP. Physics-driven CFD modeling of complex anatomical cardiovascular flows—a TCPC case study. *Ann Biomed Eng*. 2005;33: 284–300.
20. Cheng CP, Herfkens RJ, Taylor CA. Inferior vena caval hemodynamics quantified in vivo at rest and during cycling exercise using magnetic resonance imaging. *AJP—Heart and Circulatory Physiology*. 2003;284: H1161–H1167.
21. Hjortdal VE, Emmertsen K, Stenbog E, Frund T, Schmidt MR, Kromann O, Sorensen K, Pedersen EM. Effects of exercise and respiration on blood flow in total cavopulmonary connection: a real-time magnetic resonance flow study. *Circulation*. 2003;108:1227–1231.
22. Liu Y, Pekkan K, Jones SC, Yoganathan AP. The effects of different mesh generation methods on computational fluid dynamic analysis and power loss assessment in total cavopulmonary connection. *J Biomed Eng*. 2004;126:594–603.
23. Fogel MA, Weinberg PM, Rychik J, Hubbard A, Jacobs M, Spray TL, Haselgrove J. Caval contribution to flow in the branch pulmonary arteries of fontan patients with a novel application of magnetic resonance presaturation pulse. *Circulation*. 1999;99:1215–1221.
24. Orlando W, Shandas R, DeGroff C. Efficiency differences in computational simulations of the total cavo-pulmonary circulation with and without compliant vessel walls. *Comput Methods Programs Biomed*. 2006;81:220–227.

Online Supplement

Appendix – Flow Anatomy of the TCPC Pathways

Following is a series of plates detailing the flow fields for each patient geometry studied. The flow conditions are labeled as follows: “MRI” for the baseline flow condition measured by MRI through-plane velocity mapping, “EX-2” for the total caval flow of 2x baseline exercise condition, and “EX-3” for the 3x baseline exercise condition. All plots are for the MRI-measured pulmonary flow splits.

There are three types of plots presented:

Streamline plots show the tangents to the velocity vectors for flow through the TCPC. As these are steady-state simulations, they can be viewed as the path of a blood cell originating from a given place on the boundary of the caval vessels as it travels through the TCPC. IVC streamlines are color coded in red and orange, right SVC in blue and green, and left SVC in purple and pink. Azygous vein flow exists in one model, Chop20, and is color coded with light blue and green.

Pressure surface contour plots color encode hydrostatic pressure at the geometry surface. All scales shown are in mmHg and go from a high pressure encoded in red of 0 mmHg, to a negative low pressure encoded in blue in order to graphically display the pressure drop distribution through the geometry. Arrows in any of these plots correspond to the blood flow direction.

Finally, the power dissipation plots color encode volumetric power dissipation in units of mW/dm^3. Some plots are shown for a plane through the geometry superimposed on the complete geometry. These plots also show the velocity vectors for that plane. Other geometries are better illustrated with surface dissipation plots, since for some models with less flow collision, most dissipation occurs at the vessel walls.

We believe these plates add significant value to the research presented here, allowing visualization of a wide variety of patient geometries at different physiologic flow conditions representing rest and different levels of exercise. They effectively illustrate the variety of flow patterns in TCPC geometries and their effect on power dissipation.

Despite the variety of geometries presented, themes recur: 1) IVC baffle and LPA narrowings that dissipate little power at baseline flows may be sources of significant power loss at increased flows, 2) flow collision between SVC and IVC flows can be a significant source of power loss and usually increases significantly with increasing power loss, 3) increased skewing of the IVC flow toward the LPA wall in exercise flow conditions results in higher power loss. These phenomena underscore the importance of studying exercise flows in order to fully characterize the TCPC geometry.

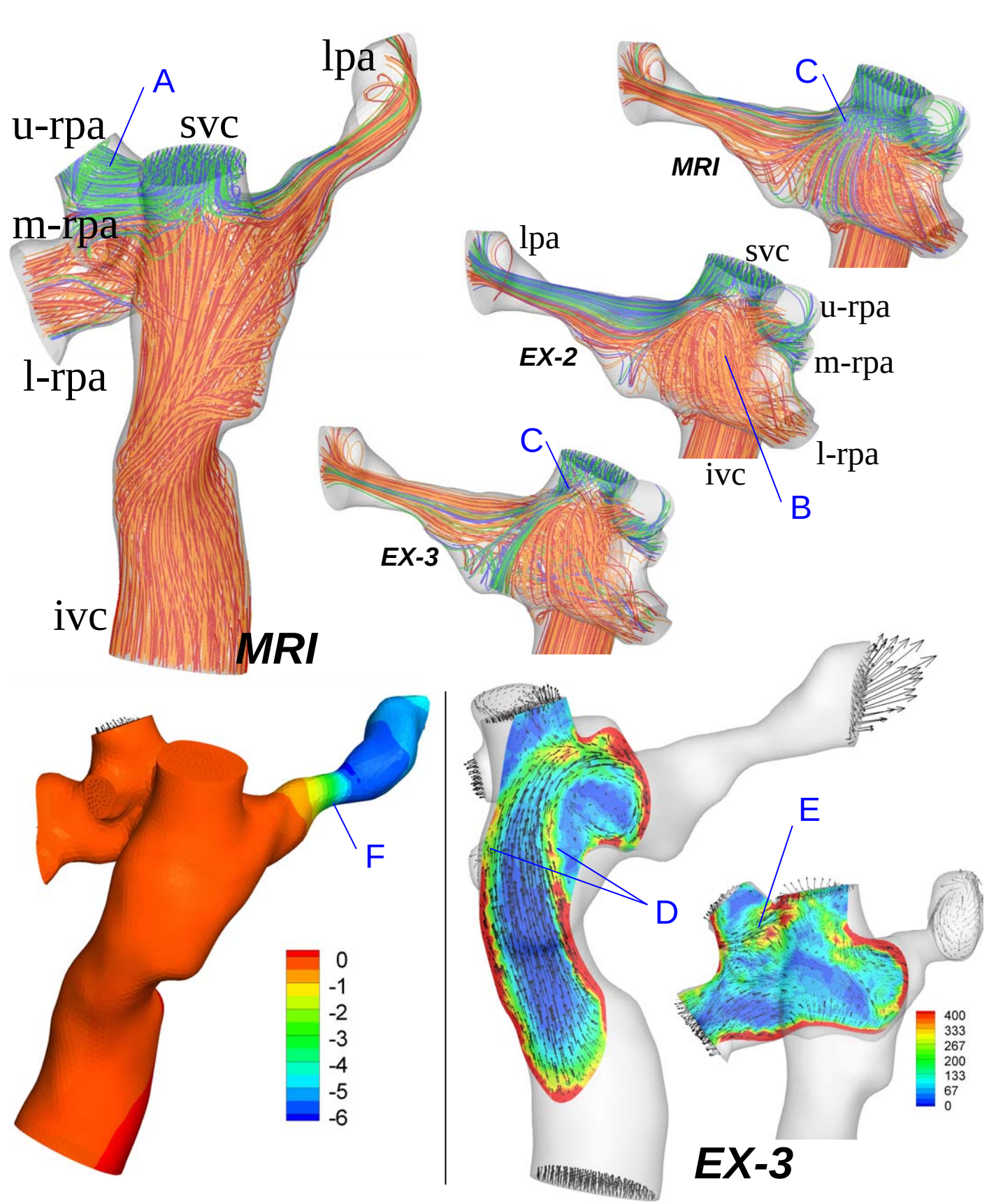

PLATE 1 Intra-cardiac TCPC with diffuse LPA hypoplasia, CHOP18. Flow through all three main RPA branches are also simulated and displayed here due to their proximity to the TCPC (A) SVC flow prefers the RPA upper lobe (B) A posterior view illustrates how the IVC flow is distributed in the connection to both lungs (good hepatic flow mixing). (C) IVC flow dominates the posterior TCPC wall and recirculates into the SVC at exercise. (D) Dissipation source shed from the baffle wall due to jet-like IVC flow. (E) Complex RPA flow between IVC-SVC generating internal hydrodynamic dissipation. (F) Moderate LPA stenosis pressure drop.

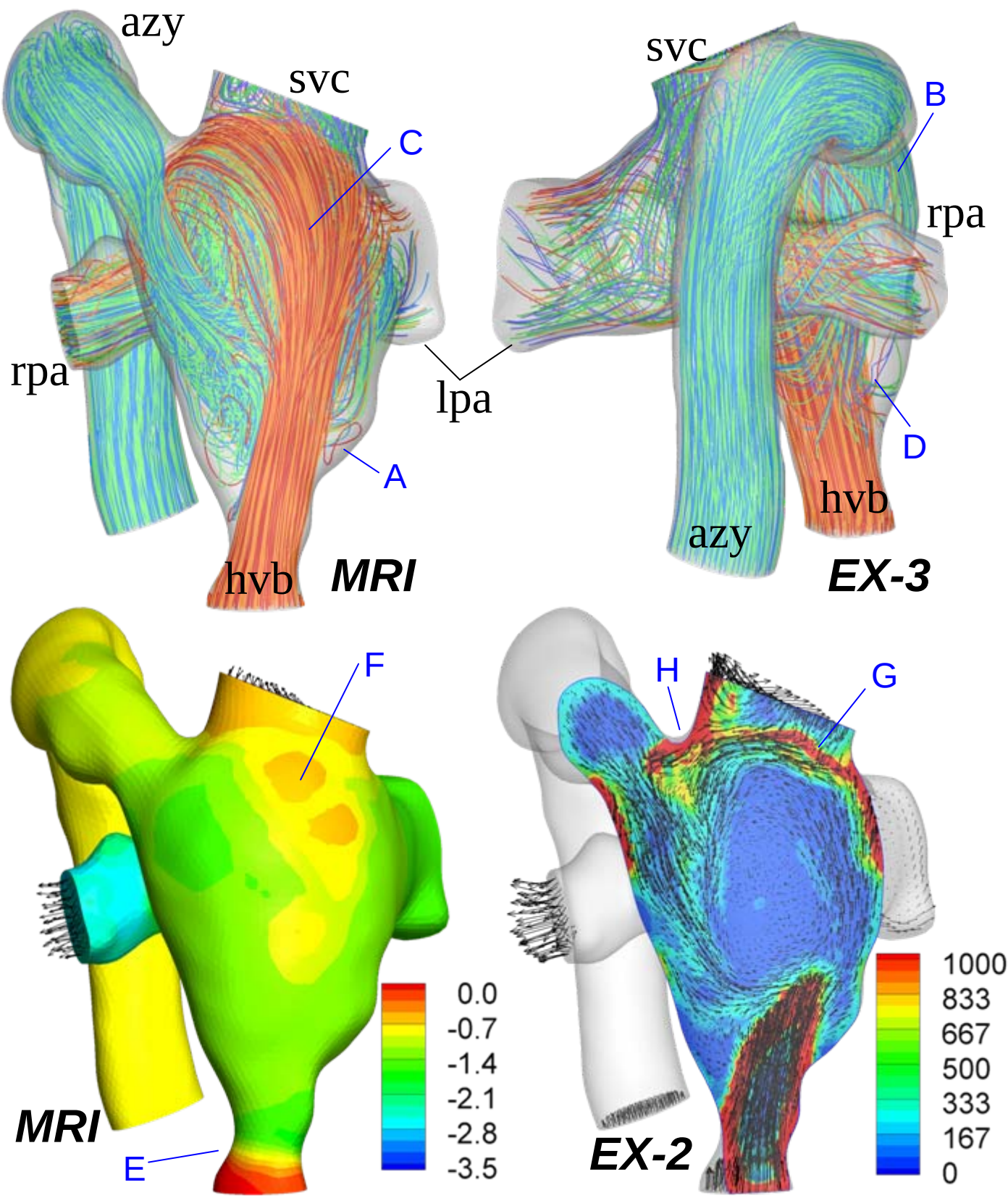

PLATE 2 Intra-atrial with azygous vein continuation, CHOP20. (A) Recirculation due to sudden area change close to the IVC inlet. (B) Azygous inflow dominates the connection proximal to the RPA. (C) It also opposes the hepatic vein baffle (hvb) inflow, deflecting it anteriorly. (D) SVC flow finds its way deep into the hvb anastomosis at the highest CO. (E) High pressure drop at the hvb narrowing. (F) Pressure increase due to stagnating hvb inflow. (G) Dissipation source along the SVC-hvb shear layer. (H) Dissipation source due to squeezed hvb stream and azygous shear layers.

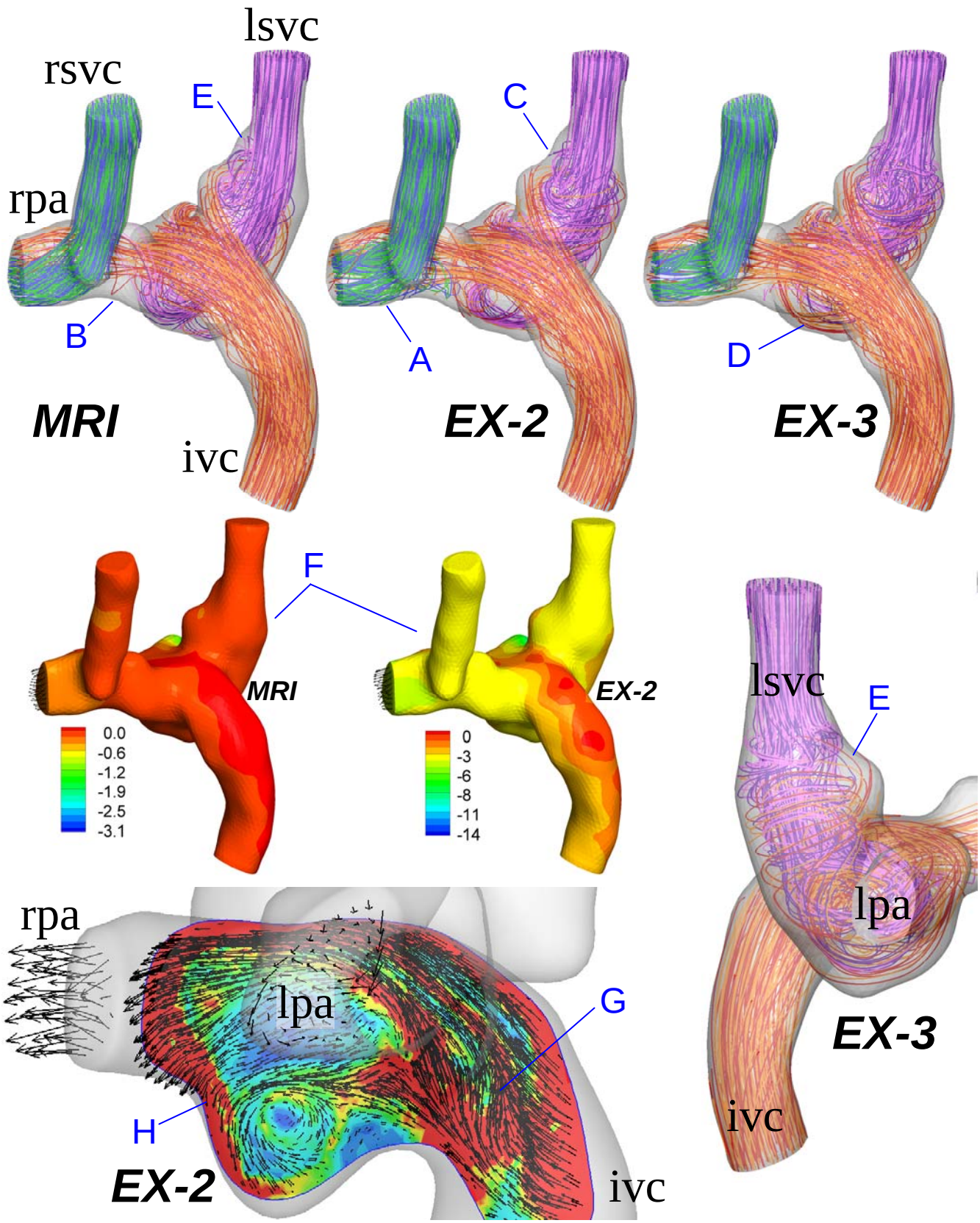

PLATE 3 Bilateral SVC with a large cambered intra-atrial conduit and end-to-side anastomosis proximal to the LSVC, CHOP22. (A) RSVC preferentially streams to RPA at all conditions. (B) Relatively stagnant region only IVC flow. (C) Considerable mixing of LSVC with IVC at the pouch. (D) Large recirculation region of LSVC pouch is more pronounced (contributed by increased IVC flow) at exercise. (E) IVC flow penetrates into LSVC – even at the resting condition. (F) At rest connection pressure is more uniform but at exercise gradients become more apparent. (G) Dissipation source type-I, squeezed IVC flow at the posterior wall. (H) Dissipation source type-II, complex shear layers of LSVC-IVC mixing.

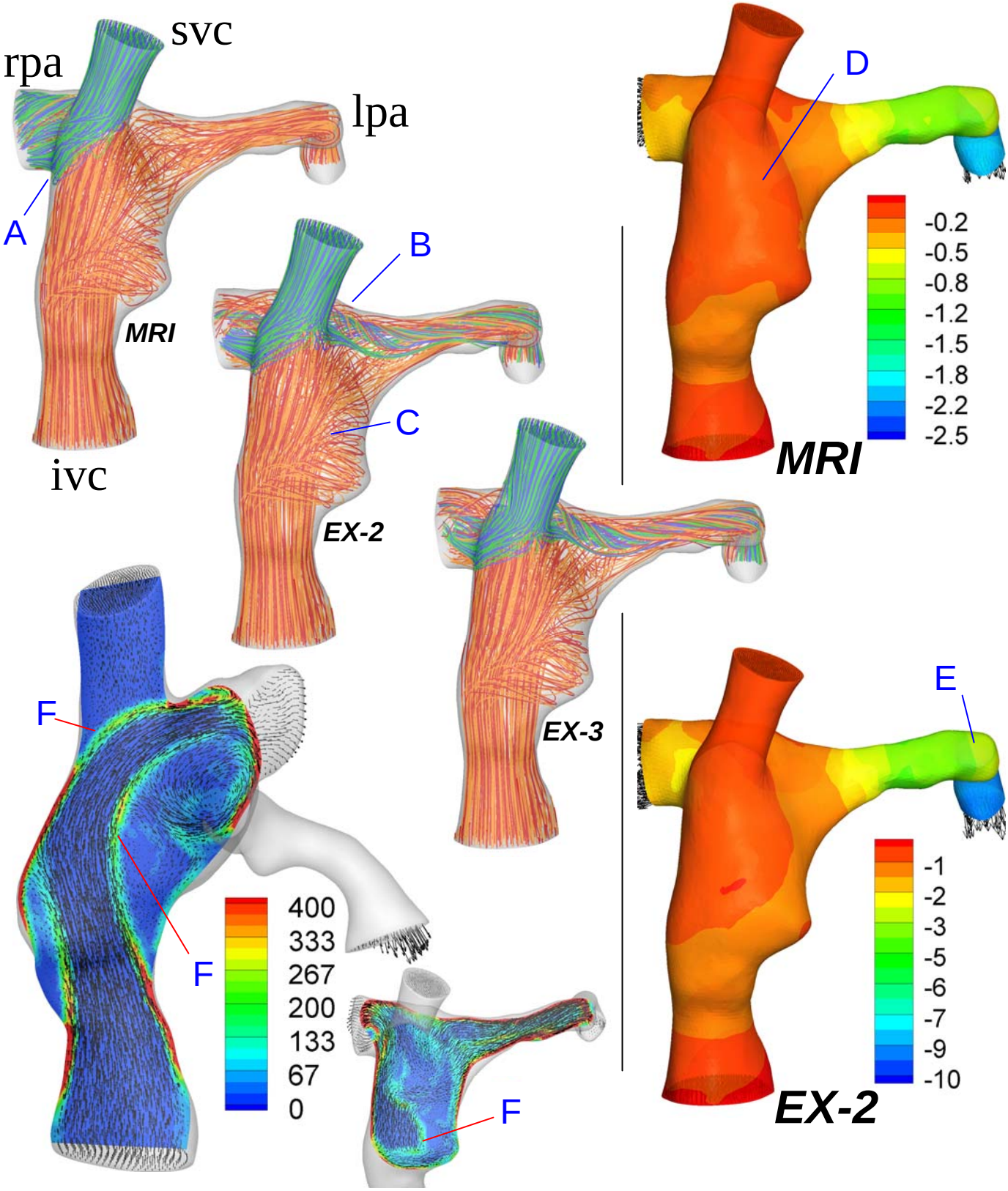

PLATE 4 A typical intra-cardiac TCPC with mild LPA hypoplasia, CHOP25. (A) SVC prefers RPA, similar to CHOP18. (B) Model has a small pouch posterior to IVC (not shown) helps to distribute IVC blood uniformly. (C) Line of reattachment, very high recirculation of the IVC blood (D) Relatively uniform pressure distribution in the connection at low cardiac outputs. (E) An almost 90 degree bend in LPA, contributing to pressure drop. (F) High internal hydrodynamic dissipation source due to emerging IVC flow.

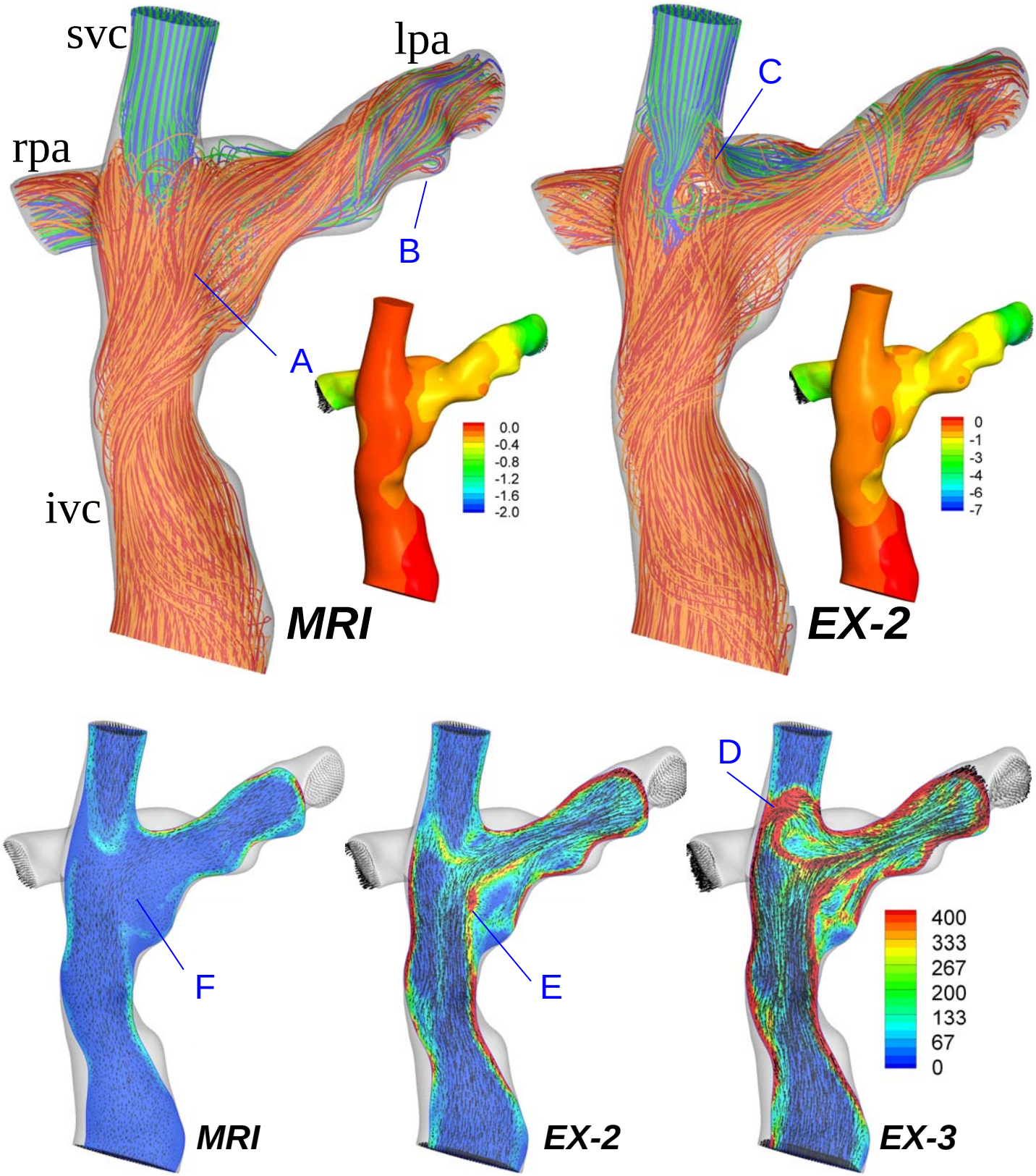

PLATE 5 Intra-cardiac TCPC, CHOP30. (A) IVC flow diverted anteriorly. (B) Small recirculation region at LPA due to irregularities. (C) IVC flow penetrates into SVC, making a posterior turn. (D) Dissipation source originating from the shear layer between colliding IVC and SVC flows. (E) Jet-like IVC flow due to sudden area increase sheds a concentrated dissipative sheet. (F) Quieter flow at the resting condition with minimal internal hydrodynamic power loss.

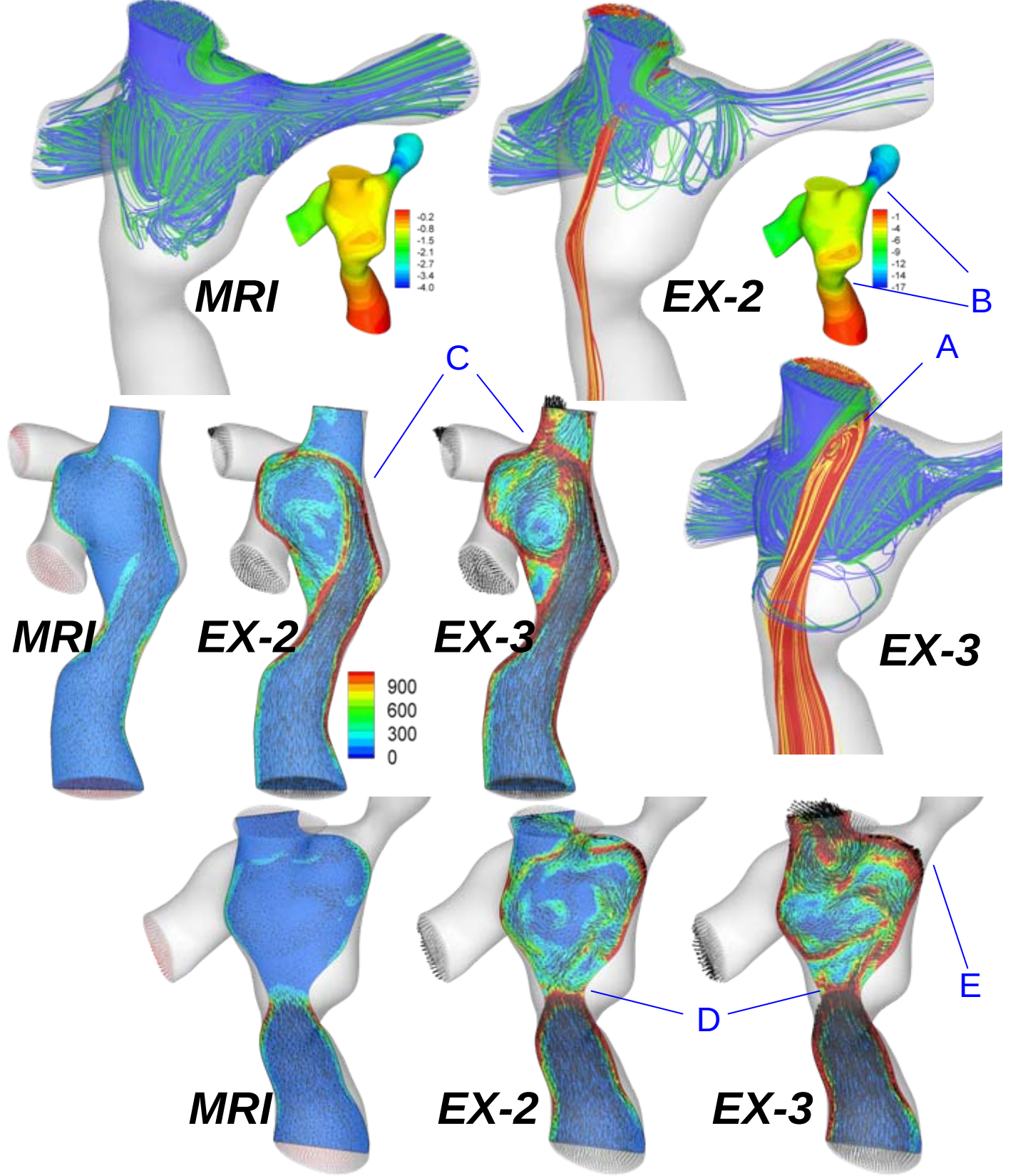

PLATE 6 Intra-atrial IVC baffle with mild narrowing, mild proximal LPA stenosis, CHOP31. (A) IVC flow with increasing penetrance into SVC with increasing flow rate. (B) Increasing pressure drop at IVC and LPA. (C) Dissipation source caused by shear layer from colliding SVC and IVC flow – minimal at rest, significant at exercise conditions. (D) Dissipation source due to IVC pinching, also mild at rest but significant at exercise. (E) Dissipation source due to LPA narrowing partially seen in this plane.

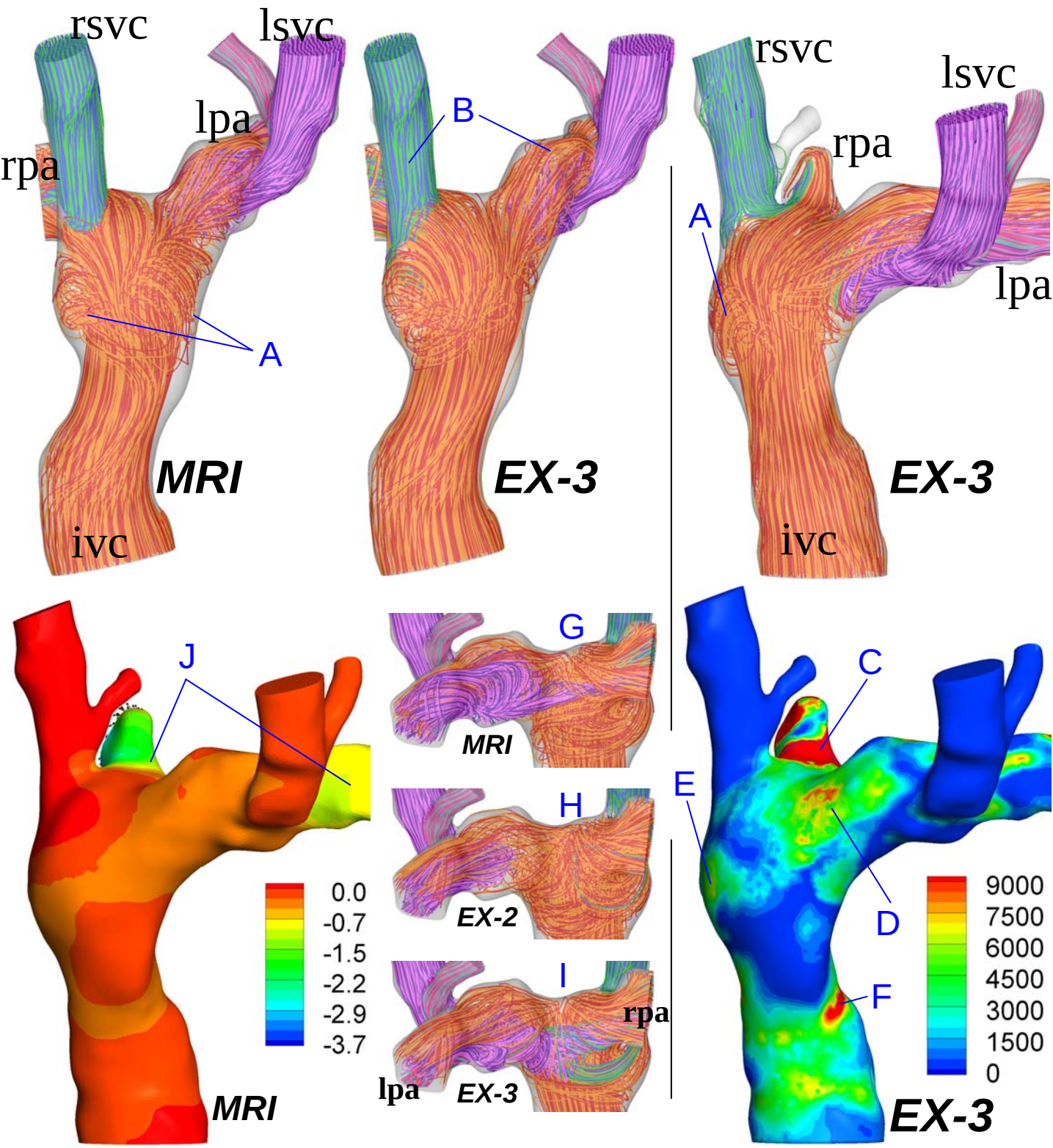

PLATE 7 Bilateral SVC's with straight IVC baffle anastomosis proximal to RSVC, CHOP32. (A) IVC flow stagnates and bifurcates into two swirls. (B) L-R SVC preferential to L-R PA's respectively; slight mixing occurs at high CO, see I. (C) Surface dissipation source at RPA due to squeezed flow towards cephalic direction. (D) Dissipation source due to IVC stream that goes to LPA without circulating. (E) Dissipation source due to circulating IVC flow. (F) Dissipation source due to area change. (J) Sudden pressure drop just downstream of LPA and RPA, associated with turning (G to I) Looking from posterior, illustrates levels of bilateral SVC flow mixing and stagnation.

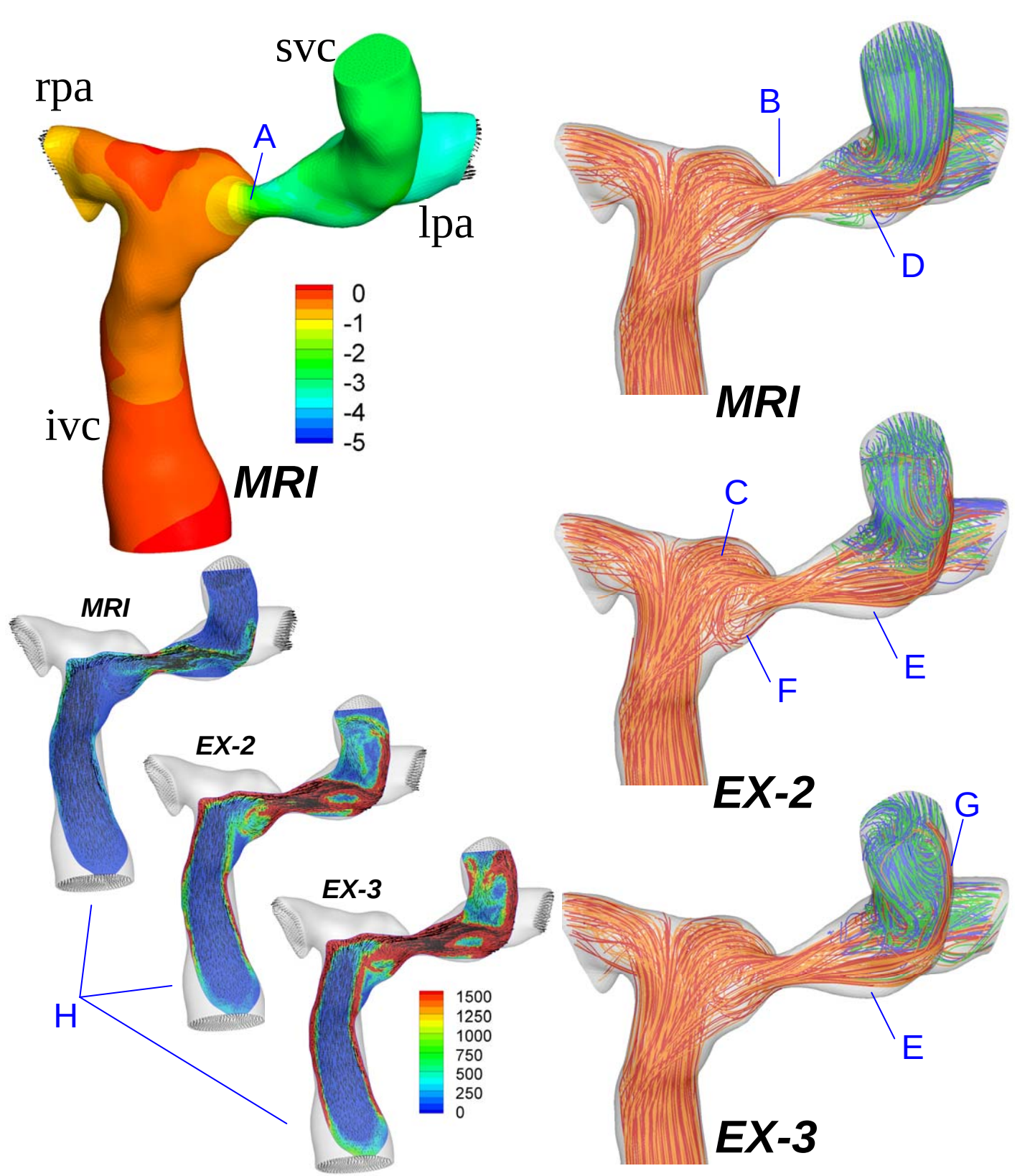

PLATE 8 Extra-cardiac TCPC with an unusual large caval offset, CHOP33. (A) Severe stenosis causing very high pressure drop which increase drastically with exercise (~20x at EX-3) In no other model is the increase in pressure drop that severe. (B) Stenosis between the cavae restricts IVC flow, largely separating the two flows. (C) IVC blood goes posterior and swirls before going through the stenosis towards the LPA. (D) SVC flow is almost exclusively directed to the LPA. (D,E) SVC flow shifted even more towards LPA with the increasing IVC flow during leg exercise. (F) Recirculation due to turning flow upstream of stenosis, becomes chaotic at the highest CO condition. (G) As observed in other models, IVC still prefers to go deep into the SVC and recirculates before going to the LPA - lesser in the resting condition. (H) Increasing dissipation sources from rest to exercise.

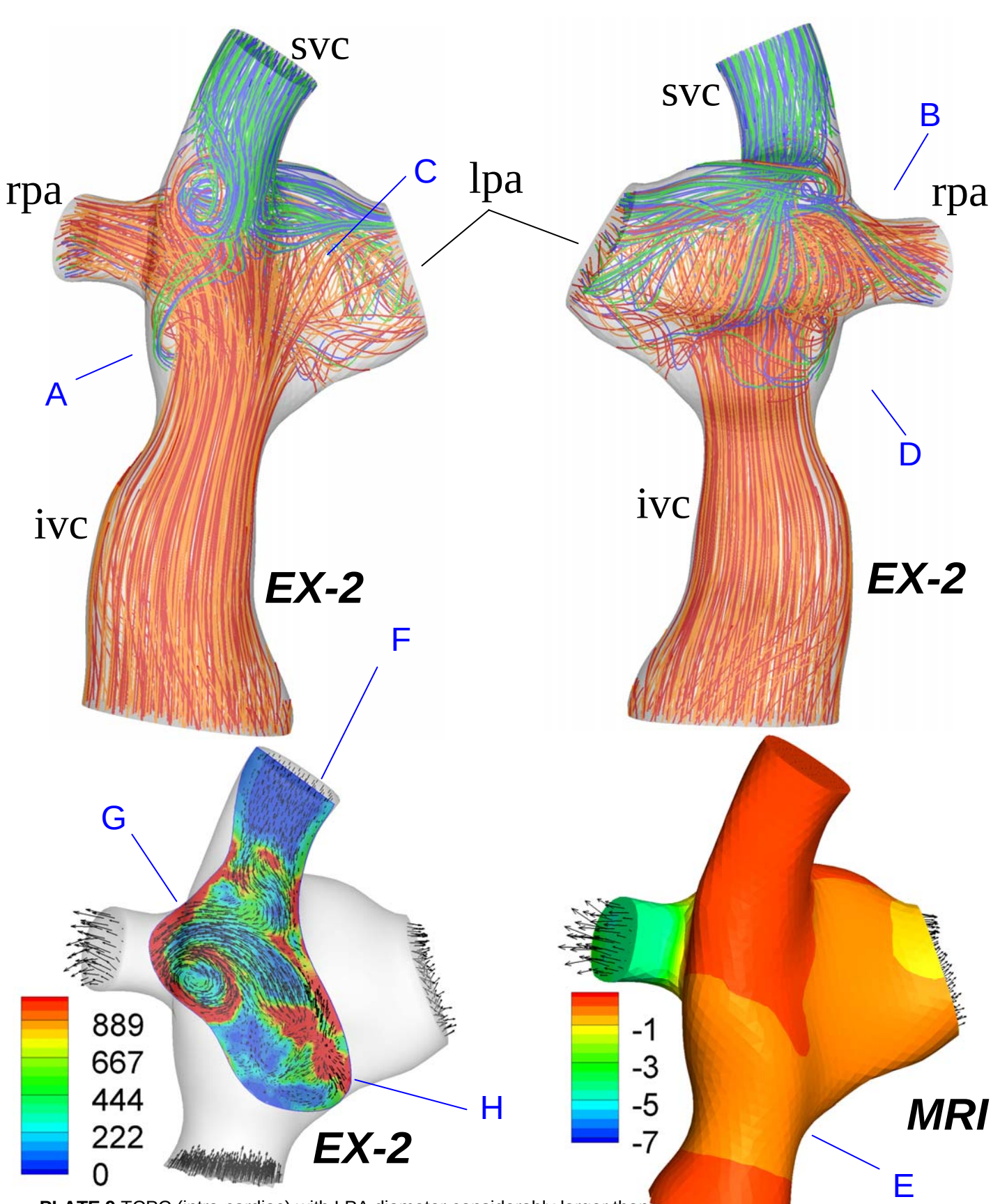

PLATE 9 TCPC (intra-cardiac) with LPA diameter considerably larger than the RPA, CHOP34. (A) Recirculation due to sudden area change close to the IVC inlet. (B) Azygous inflow dominates the connection proximal to the RPA. (C) It also opposes the IVC inflow deflecting it towards the anterior. (D) SVC flow finds its way deep in to the IVC anastomosis at the highest CO. (E) Pressure drop at the IVC narrowing. (F) Pressure increase due to stagnating IVC inflow. (G) Dissipation source along the SVC-IVC shear layer. (H) Dissipation source due to squeezed IVC stream and azygous shear layers.

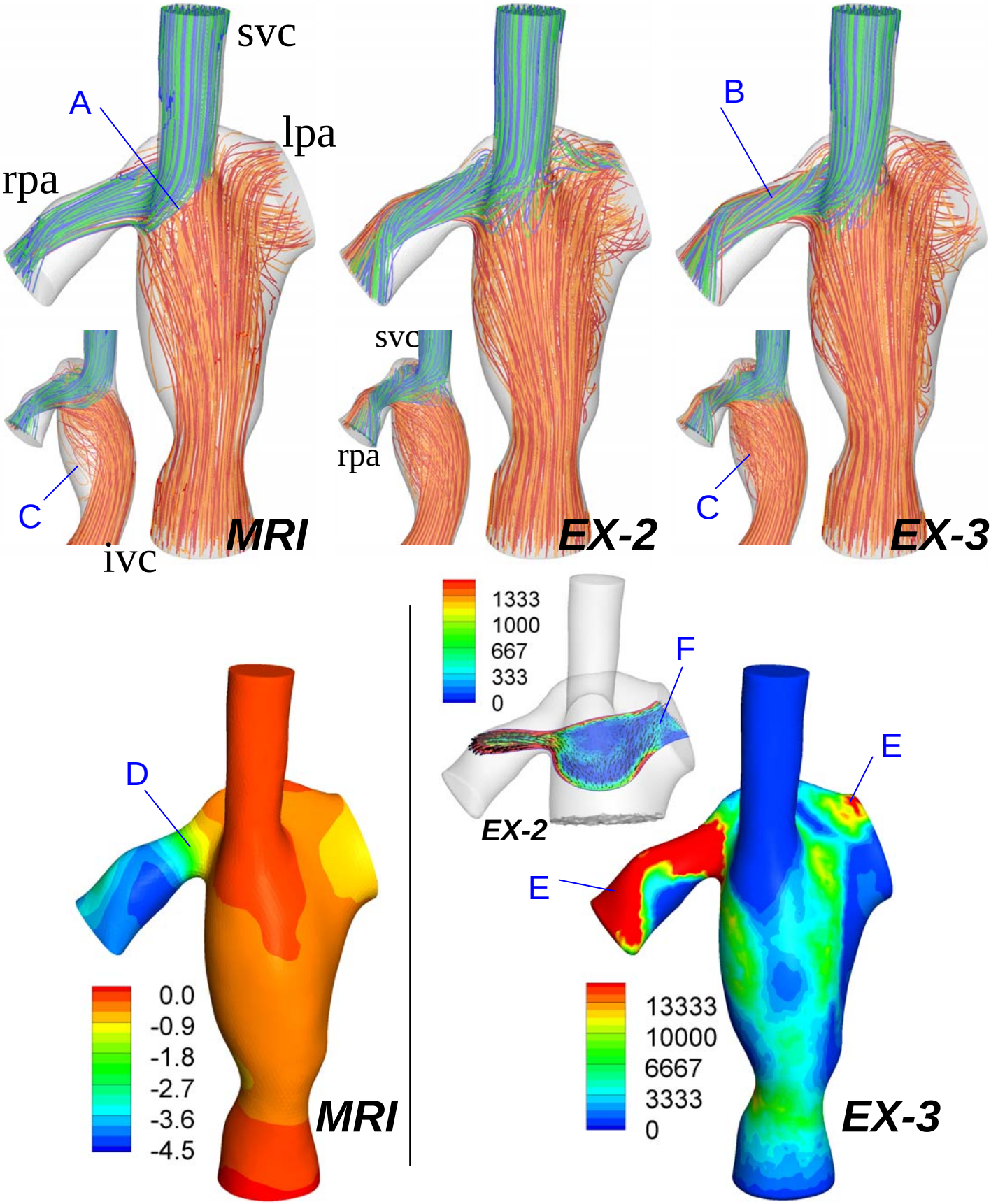

PLATE 10 Intra-cardiac TCPC with larger LPA than RPA, CHOP37. (A) Sharp SVC-IVC flow interface which is more diffuse with exercise (B) SVC flow prefers right lung, only at EX-2 there is slight flow towards the left lung (C) Another view looking from RPA shows the recirculating IVC flow in the pouch region; shape of recirculation changes from rest to exercise (D) Pressure drop at RPA. (E) Typical dissipation sources on the PA vessel walls due to squeezed flow in that region. (F) Internal sources of dissipation along an arbitrary cut.